Numerical prediction of fully-suspended slurry flow in horizontal pipes

Gianandrea Vittorio Messa [a], Michael Malin [b], Stefano Malavasi [a,*]

[a] Dipt. I.C.A., Politecnico di Milano, Piazza Leonardo da Vinci, 32, 20133 Milano, Italy
[b] CHAM Limited, Bakery House, 40 High Street, Wimbledon, London SW19 5AU, UK

Article history:
Received 18 March 2013
Received in revised form 20 December 2013
Accepted 1 February 2014
Available online 10 February 2014

1. Introduction

Pipe flows of solid–liquid mixtures in the form of slurry are commonly encountered in many applications, in the field of both civil and industrial engineering. Pressure gradient and concentration distribution have been the most serious concern of researchers, as they dictate the selection of pump capacity and may be used to determine parameters of direct importance (mixture and solid flow rates) as well as secondary effects like wall abrasion and particle degradation.

The flow of solid–liquid mixtures is very complex. Doron and Barnea [1] identified the flow patterns that characterize the flow of slurries through horizontal pipes. If the flow rate is sufficiently high, turbulence is effective in keeping all the solids suspended (fully suspended flow); otherwise the particles accumulate at the pipe bottom and form a packed bed, either sliding (flow with a moving bed) or not (flow with a stationary bed). The transitions between flow patterns are not always clear and they are usually identified by post-processing measured data in terms of solid–volume-fraction profile and pressure gradient [2]. In particular, the transition between fully-suspended and bed flows corresponds to a minimum in the plot of pressure gradient versus slurry superficial velocity (which is the ratio between the volumetric flow rate of the two-phase mixture and the area of the pipe section), qualitatively depicted in Fig. 1. The threshold velocity between the two regimes is usually referred to as the deposition velocity. Several correlations – usually of an empirical nature – have been developed for roughly estimating the deposition velocity: an overview is reported by Albunaga [2] and Pecker and Helvaci [3]. As an example, the formula of Wasp [4], which is one of the simplest and most frequently cited in the literature, is given below:

$$V_D = 4\left(\frac{d_p}{D_p}\right)^{1/6} C^{1/5}\sqrt{2|\mathbf{g}|D_p\left(\frac{\rho_p}{\rho_f}-1\right)} \tag{1}$$

where: V_D is the deposition velocity; d_p is the particle size; D_p is the pipe diameter; C is the delivered solid volume fraction; $\mathbf{g}$ is the gravitational acceleration; and ρ_f and ρ_p are the density of the fluid and particles respectively.

The present work focuses on fully-suspended flow, and so the considerations reported below hold when turbulence is effective in keeping all the solids suspended. The pressure gradient of the solid–liquid slurry is generally higher than that of an equal flow rate of pure liquid because the particles produce additional dissipation. Actually, the way in which the particles affect the dissipation is a very complex matter, and under specific flow conditions, either negligible variations or even a decrease in losses with respect to the single-phase case was observed [5]. However, this eventuality was not considered here, because it is very rare and pronounced only for vertical pipe flows. The frictional loss of the two-phase flow is considered as a combination of viscous friction and mechanical friction [2,3,6]. The former is due to the liquid viscosity in the laminar sublayer, and is not affected by the solid particles unless they are fine enough to be trapped within the laminar sublayer, which is not the case here. The latter is due to particle–wall interactions which are the result of the dispersive action of both turbulence and particle

* Corresponding author. Tel.: +39 02 2399 6261.
E-mail addresses: gianandreavittorio.messa@polimi.it (G.V. Messa), mrm@cham.co.uk (M. Malin), stefano.malavasi@polimi.it (S. Malavasi).

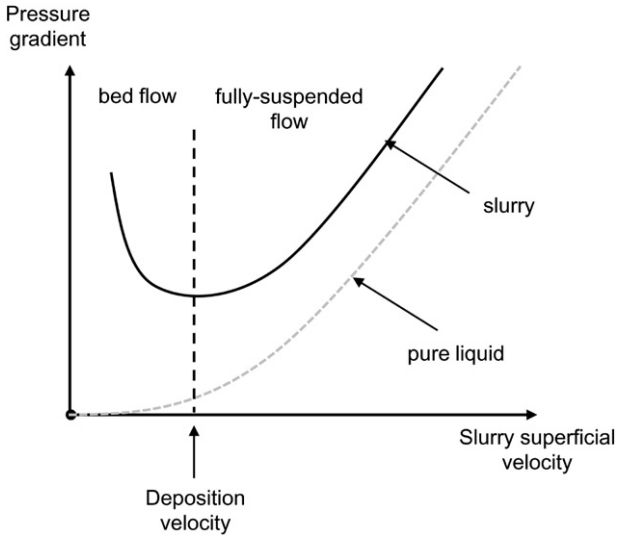

Fig. 1. Qualitative plot of pressure gradient versus slurry superficial velocity. The curve for an equal flow rate of pure liquid is depicted too.

collisions. Some authors have argued for the existence of a hydrodynamic lift force to account for the repulsion of particles from the pipe wall observed in some experiments, which is accompanied by a decrease of the mechanical friction [7]. Wilson and co-workers [8,9] developed a model to account for this effect, but the global nature of its formulation precludes its implementation in a CFD code.

The distribution of the delivered solid volume fraction over the pipe section shows a gradient along the vertical direction arising from gravitational stratification. Fully-suspended flows in which this gradient is clearly detectable are referred to as heterogeneous flows [1]. Conversely, if the slurry superficial velocity is very high, and the effect of gravity is negligible compared to drag and turbulent dispersion, the solid volume fraction can be regarded as uniformly distributed (pseudo-homogeneous flow). Whatever the flow pattern, the solid volume fraction distribution is usually quantified by means of its characteristic vertical profile, which according to the kind of instrumentation used to perform the measurements, is either the profile along the vertical diameter (Fig. 2(a)) or the chord-averaged profile (Fig. 2(b)). Since the variation of the solid volume fraction along each horizontal chord is likely to be small, the two profiles are generally close to each other.

The axial velocity distribution is not univocally defined for a two-phase flow, since it may be represented in terms of either the fluid velocity, the particle velocity, or the mass-averaged mixture velocity. Whatever velocity is considered, unlike that of a single-phase flow, the axial velocity distribution of a solid–liquid mixture is asymmetric with respect to the pipe axis, and the maximum value is shifted towards the upper wall. This behavior was interpreted by Ling and co-workers [10] as a consequence of the fact that, due to the effect of gravity, the slurry density in the lower part of the pipe is higher than that in the upper part. As a result, the fluid spends more energy to drive the particles in the lower part, resulting in a lower slurry velocity in that area. Actually, the asymmetry of the velocity profile is almost undetectable for pseudo-homogeneous flows.

Numerous experimental investigations have been carried out to determine pressure gradients, volume fraction distributions, and less frequently, velocity profiles of slurry flows in horizontal pipes. The dispersed phase is usually sand [6,11–17], but spherical glass beads [18–20], ash [21] and solid nitrogen particles [22,23] have also been considered.

The experimental determination of solid volume fraction and velocity presents considerable technical difficulties. Local values of solid volume fraction can be measured by isokinetic probe sampling, but these techniques may produce significant errors near both the pipe wall [24] and the pipe axis [12]. More accurate results – but with uncertainties of a few percent – are obtained using expensive gamma-ray density gauges, which are used to determine chord-average values of solid volume fraction. The mean concentration of the slurry is characterized in different ways by researchers. Kaushal and Tomita [18,20] and Kaushal et al. [19] considered an overall area-average concentration, evaluated by integrating the local volume fraction profile measured by an isokinetic sampling probe. Matousek [7,13] measured the mean delivered concentration in the pipeline by a counter flow meter. Other authors [14,15] reported values of the mean in-situ concentration, obtained by adding weighted quantities of solids to the loop, whose volume was known. In all cases, the uncertainty about this parameter must be considered when making reference to literature data.

Local values of velocity in slurry flows are commonly measured by the electrical probe developed at the University of Saskatchewan [25] or, less frequently, by Laser Doppler Velocimetry. The former method allows detecting the velocity of the particles, and the main limitation is that the measurements may be affected by the distortion in the flow field produced by the probe, especially close to the pipe walls. The latter method is capable of providing the fluid and particle velocities, but specific procedures are required for discriminating between the two velocities. Numerous examples of applying LDV for solid–liquid flows are reported in the literature [26], but the technique is claimed to be unreliable for concentrated mixtures (mean delivered solid concentration above 15–20% by volume) except homogeneous flows in which the difference in velocity between the phases is small [27].

Simplified models have been developed based on a global formulation to predict macroscopic parameters like the pressure gradient for all flow configurations. The equivalent liquid models apply in the case of fully-suspended flows [3,7], while two- and three-layer models [28–33] may be employed for flows with moving bed and stationary

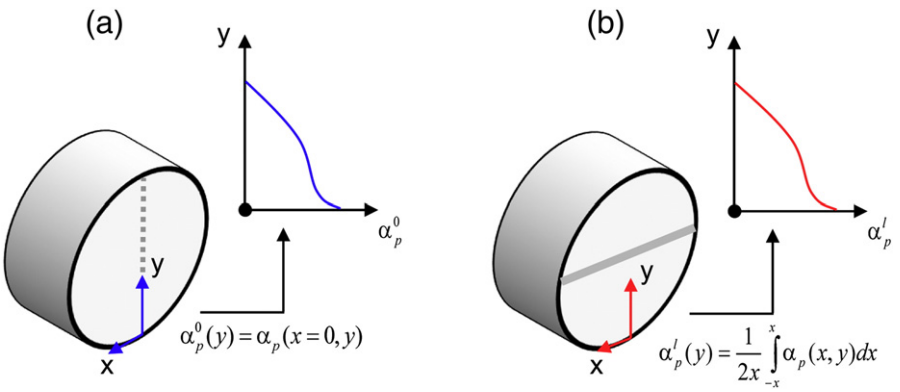

Fig. 2. Solid volume fraction distribution: (a) values along the vertical diameter and (b) chord-averaged profile.

deposit, respectively. Improved versions have been proposed to account for the presence of multi-sized particles [21], the influence of particle shape [14], the additional stresses due to particle–wall interactions [3], and the already-mentioned repulsion of particles from the wall observed in some experiments [9]. Using those models, the pressure gradient can be estimated easily, and the predictions agree with the experimental evidence over a wide range of operating conditions. Therefore, these models represent a very powerful tool for most engineering applications. However, their global formulation makes them unsuitable for predicting the solid–volume-fraction and velocity distributions, which require the development and validation of distributed models that can also be applied to more complex geometries.

CFD has been widely used to investigate solid–liquid pipe flows, but there is a need for the development of a model that is both reliable and computationally economical, and therefore attractive to engineers. The majority of existing CFD models employ an Eulerian–Eulerian approach, since Eulerian–Lagrangian models are not applicable to dense mixtures due to their excessive computational cost. Some workers studied the problem by means of the Algebraic Slip Model (ASM), which solves the momentum equation for the mixture rather than for both phases, thereby saving computational time. However, the ASM assumes that local equilibrium is achieved between the phases over short spatial length scales, so that it can be used only for very low values of the Stokes number. Also when applicable, the ASM proved inadequate to estimate the pressure drop even for fully-suspended flows [33], and it doesn't seem very accurate in predicting the solid volume fraction distribution [10,33]. Most authors made use of an Eulerian two-fluid model with closures derived either from empirical or semi-empirical relations [34], or from the Kinetic Theory of Granular Flow (KTGF) [22,23,33,35–37]. Anyway, even for pipe flows, the existing two-fluid models show some problems which may complicate their application to more complex flows of engineering interest. The first impression is that these models are easily susceptible to numerical instabilities, which often results in solutions characterized by non-physical asymmetry [33] or oscillations [37]. In some cases, the simulations are very time-consuming; for example, Ekambara et al. [36] attained a stable steady-state solution performing a U-RANS simulation and then averaged the solution over a considerable time interval. A similar procedure may not be easily applicable when dealing with complex geometries, since the calculation time would probably become prohibitively expensive. In other cases, the validation of these models with respect to the experimental evidence is often rather poor, in the sense that the comparison is either limited to a few flow conditions [33,35] or highlights an occasionally excellent capacity of the model to describe adequately the main features of the flow [37]. It is worth noticing that none of the existing models proved unquestionably capable of detecting the minimum in the pressure gradient versus slurry velocity, which characterizes the transition to bed flows [23,35].

In this work a mathematical model is presented for the prediction of fully-suspended flows in horizontal pipes, which is based on an Euler–Euler approach that uses the Inter-Phase Slip Algorithm (IPSA) of Spalding [38,39]. The proposed model shows comparable or better agreement with the experimental evidence than similar models [33,35–37], and it also overcomes the main limitations inferred from inspection of these earlier papers, namely susceptibility to numerical instability and high computational cost. In fact, the new model requires relatively low computer time to attain a converged steady-state solution and is capable of providing a numerical solution without unphysical asymmetries or oscillations. The novelty of the proposed model, which is the basis for its good performance, resides in the combined use of modeling strategies previously developed but never employed simultaneously to the flows considered in this paper: phase diffusion fluxes are introduced in all conservation equations to reproduce the effect of the turbulent dispersion of particles; the presence of other particles on the interfacial momentum transfer is taken into account by considering their effect on a mixture viscosity; a wall function is employed to model the mechanical contribution to the wall shear stress.

In the interests of guaranteeing the widest possible applicability, the model predictions of the main features of the flow (pressure gradient, and solid-concentration and velocity distributions) are validated with respect to various sets of experimental data [7,11,13–15] over a large range of operating conditions, in terms of pipe diameter (50 to 150 mm), grain material (glass beads and sand), particle size (90 to 520 μm), slurry superficial velocity (1 to 7 m/s), and mean delivered solid concentration up to 40% by volume of mixture. The uncertainties of both computations and measurements are discussed when comparing the numerical results with those of the experiment.

2. Mathematical model

2.1. Conservation equations

The two-phase flow is represented by using an Eulerian approach in which both phases are treated as interpenetrating continua. The flow is assumed to be statistically steady in the sense that Reynolds-averaging has been applied, and so the continuity equation for phase $k = f, p$ takes the following form:

$$\nabla \cdot (\alpha_k \rho_k \mathbf{U}_k) = \nabla \cdot (\rho_k D \nabla \alpha_k) \tag{2}$$

where: α_k is the volume fraction; ρ_k is the density; $\mathbf{U}_k$ is the velocity vector; and D is a phase diffusion coefficient, which appears in the phase diffusion term that represents the turbulent flux associated with correlations between fluctuating velocity $\mathbf{u}_k'$ and volume fraction α_k'. These correlations, which appear in all conservation equations, are modeled in terms of a gradient-diffusion approximation in which the phase-diffusion coefficient D is the same for both phases and is given by:

$$D = \frac{\nu_{t,f}}{\sigma_\alpha} \tag{3}$$

where $\nu_{t,f}$ is the turbulent kinematic viscosity of the carrier fluid phase, determined by turbulence modeling; and σ_α is the turbulent Schmidt number for volume fractions. The origin of the correlations $\overline{\mathbf{u}_k' \alpha_k'}$ in all conservation equations has been clarified elsewhere [40] and their modeling by means of a gradient diffusion approximation with diffusivity given by Eq. (3) is a well known approach in the literature. The turbulent Schmidt number for volume fractions may in some sense be interpreted as the ratio of turbulent momentum transport to the turbulent transport of phase mass. However, the numerical value of σ_α is not well established in the literature because no single constant value can be used to match the various sets of experimental data [41,42]. These values typically fall in the range 0.2 to 0.9. In the proposed model, we set the turbulent Schmidt number for volume fractions equal to 0.7, since this value procures the best overall agreement with the experimental evidence. The presence of phase diffusion fluxes in all conservation equations, which has the advantage of promoting numerical stability, distinguishes the present model from similar ones applied to slurry flows. The mean global continuity is given by the equation that states that the two volume fractions must sum to unity.

The momentum equation for phase $k = f, p$ is:

$$\nabla \cdot (\alpha_k \rho_k \mathbf{U}_k \mathbf{U}_k) = -\alpha_k \nabla P + \nabla \cdot \left[\alpha_k \left(\boldsymbol{T}_k + \boldsymbol{T}_{t,k}\right)\right] + \alpha_k \rho_k \mathbf{g} + \mathbf{M}_k + \nabla \cdot (\rho_k D \mathbf{U}_k \nabla \alpha_k) \tag{4}$$

where: P is the pressure, shared by the phases; $\boldsymbol{T}_k$ and $\boldsymbol{T}_{t,k}$ are the viscous and turbulent stress tensors respectively; and $\mathbf{M}_k$ is the generalized drag force per unit volume, which will be discussed later. The viscous stress tensor (present only in the fluid phase) and the turbulent stress tensor (present in both phases) are given by:

$$\boldsymbol{T}_f = 2\rho_f \nu \boldsymbol{D}_f \qquad \boldsymbol{T}_{t,k} = 2\rho_k \nu_{t,k} \boldsymbol{D}_k \tag{5}$$

where: ν is the kinematic viscosity of the fluid, $\nu_{t,k}$ is the eddy viscosity, and $\boldsymbol{D}_k$ is the deformation rate tensor, equal to:

$$\boldsymbol{D}_k = 0.5\left[\nabla \mathbf{U}_k + (\nabla \mathbf{U}_k)^+\right] \tag{6}$$

where the superscript "+" indicates that the transpose of the dyadic $\nabla \mathbf{U}_k$ is taken.

The interfacial momentum transfer term accounts for the momentum transfer between phases, and is given by stationary drag, Saffman and Magnus lift, added mass, history and other forces [43]. The two-fluid model represents the turbulent dispersion of particles by means of phase diffusion fluxes in all conservation equations, including the phasic continuity equation (Eq. (1)), and so an explicit turbulent-dispersion force term makes no appearance in the momentum equation. A literature review [36,44] revealed that lift, virtual mass and history forces are negligible for the flows considered here. The results of preliminary simulations regarding different flow conditions served as further confirmation of these indications. The interfacial transfer term is therefore given by:

$$\mathbf{M}_k = \frac{3}{4d_p} C_d \alpha_p \rho_f |\mathbf{U}_r| \mathbf{U}_r \tag{7}$$

where: C_d is the drag coefficient; and $\mathbf{U}_r$ is the slip velocity between the phases, equal to $\mathbf{U}_p$–$\mathbf{U}_f$ for $k = f$ and to $\mathbf{U}_f$–$\mathbf{U}_p$ for $k = p$. The drag coefficient is given by the well known Schiller and Naumann [45] formula:

$$C_d = \max\left[\frac{24}{\mathrm{Re}_p}\left(1 + 0.15\mathrm{Re}_p^{0.687}\right), 0.44\right] \tag{8}$$

in which Re_p is the particle Reynolds number. Following Ishii and Mishima [43], in order to account for the presence of other particles, the particle Reynolds number is defined as $\mathrm{Re}_p = \rho_C d_p |\mathbf{U}_r| / \mu_m$, where μ_m is the viscosity of the mixture. Several empirical correlations for the mixture viscosity are available in the literature [46], and typically they depend on parameters that account for the shape and size distribution of the particles. In the present work, use is made of a local formulation of the Mooney [47] formula, which relates μ_m to the local solid volume fraction, α_p:

$$\mu_m = \rho_f \nu \exp\left(\frac{[\eta]\alpha_p}{1 - \alpha_p/\alpha_{pm}}\right). \tag{9}$$

Two the two fitting parameters in Eq. (9) are the maximum packing concentration α_{pm} and the intrinsic viscosity $[\eta]$. The former accounts for the shape and size distribution of the particles, as well as the shear rate. For a given set of particles, it can be measured statistically by allowing the slurry to settle in a quiescent condition, but due to the complexity of the interacting mechanisms involved when the slurry is flowing, α_{pm} is generally found as a fitting parameter, and checked against experimental findings [3]. In the present work, α_{pm} was set to 0.7, a value which lies in the range of 0.6–0.75 reported in the literature. It should be noted that lower values have been used for highly irregular-shaped particles [14]. The intrinsic viscosity was assigned a value of a 2.5 in all the simulations. This value has been well documented in the literature for spherical particles. For the first time, the mixture viscosity approach is employed in a two-fluid model for the simulation of slurry flows in pipes. In particular, the asymptotic behavior of the viscosity of the mixture, which tends to infinity as the solid concentration approaches the maximum packing one, sets an upper limit to the concentration of particles, preventing the solids from over-packing. This avoids the need to introduce a collisional pressure term in the dispersed-phase momentum equations. The absence of this term contributes to the numerical stability of the proposed model.

In the absence of an appropriate closure model, the effect of the hydrodynamic lift force is ignored in the present work. A semi-theoretical model for this force was derived by Antal et al. [48] for air–water bubbly flow in the laminar regime, but it proved unsuitable for slurry flows, confirming the observations of Ekambara et al. [36]. Conversely, the model of Wilson and co-workers [8,9] is applicable to slurry flows, but cannot be included in a CFD code due to the global nature of its formulation.

2.2. Turbulence modeling

The following modified form of the k–ε model is used for evaluating the turbulent kinematic viscosity of the carrier fluid $\nu_{t,f}$:

$$\nabla \cdot \left(\alpha_f \rho_f \mathbf{U}_f k\right) = \nabla \cdot \left[\alpha_f \rho_f \left(\nu + \frac{\nu_{t,f}}{\sigma_k}\right)\nabla k\right] + \alpha_f \rho_f (P_k - \varepsilon) + \nabla \cdot \left[\rho_f \frac{\nu_{t,f}}{\sigma_\alpha} k \nabla \alpha_f\right] \tag{10}$$

$$\nabla \cdot \left(\alpha_f \rho_f \mathbf{U}_f \varepsilon\right) = \nabla \cdot \left[\alpha_f \rho_f \left(\nu + \frac{\nu_{t,f}}{\sigma_\varepsilon}\right)\nabla \varepsilon\right] + \alpha_f \rho_f \frac{\varepsilon}{k}(C_{1\varepsilon} P_k - C_{2\varepsilon}\varepsilon) + \nabla \cdot \left[\rho_f \frac{\nu_{t,f}}{\sigma_\alpha} \varepsilon \nabla \alpha_f\right] \tag{11}$$

$$\nu_{t,f} = C_\mu \frac{k^2}{\varepsilon} \tag{12}$$

in which $P_k = 2\nu_{t,f}\boldsymbol{D}_f : \nabla \mathbf{U}_f$ is the volumetric production rate of k due to the working of the Reynolds stresses against the mean flow. The standard values [49] of the model constants are employed, namely $\sigma_k = 1.0$, $\sigma_\varepsilon = 1.314$, $C_\mu = 0.09$, $C_{1\varepsilon} = 1.44$, and $C_{2\varepsilon} = 1.92$. The form of the k–ε model turbulence model employed for the present simulations is the simplest possible extension [50,51] of the standard high-Reynolds form of the k–ε model of Launder and Spalding [49] to two-phase flows, apart from the inclusion of phase-diffusion terms, which are required for consistency with the corresponding terms in the phase continuity equations [38,51]. A rigorous mathematical derivation of the transport equations for k and ε, of which Eqs. (10)–(12) are a simplified formulation, is provided in Elghobashi and Abou-Arab [52]. In order to account for the influence of the dispersed phase on the turbulence of the continuous phase, the extra-viscosity model of Sato and Sekoguchi [53] was briefly explored but finally not employed because it was found to have no influence on the flow variables addressed in this paper.

There appears to be no simple model of general validity for evaluation of the particle eddy viscosity $\nu_{t,p}$ in dense particle flows. Nevertheless, even the simple model of $\nu_{t,p} = \nu_{t,f}$ indicated by Issa and Oliveira [54] was found to yield accurate predictions of those features of slurry flows which are of the most engineering interest, namely pressure gradient, solid volume fraction distribution, and velocity distribution. No significant variation was observed when employing the other algebraic models listed in Messa [46].

2.3. Computational domain and boundary conditions

The computational domain is shown in Fig. 3, where it is evident that flow and geometrical symmetry about the vertical axis [11,19] have been exploited by solving only over one half of the pipe section. At the pipe inlet, the following variables are imposed: the mass fluxes of both phases, $\rho_f \alpha_f^{in} u_{z,f}^{in}$ and $\rho_p \alpha_p^{in} u_{z,p}^{in}$; the mean axial velocities of the two phases, $u_{z,f}^{in}$ and $u_{z,p}^{in}$; the turbulent kinetic energy, k^{in}; and its dissipation rate, ε^{in}. The distributions of $u_{z,f}^{in}$, $u_{z,p}^{in}$, k^{in}, and ε^{in} are obtained from the boundary-layer theory of Prandtl and Nikuradse [55] for fully-developed single-phase flows in straight pipes. No slip is assumed between the phases at the inlet section, and therefore

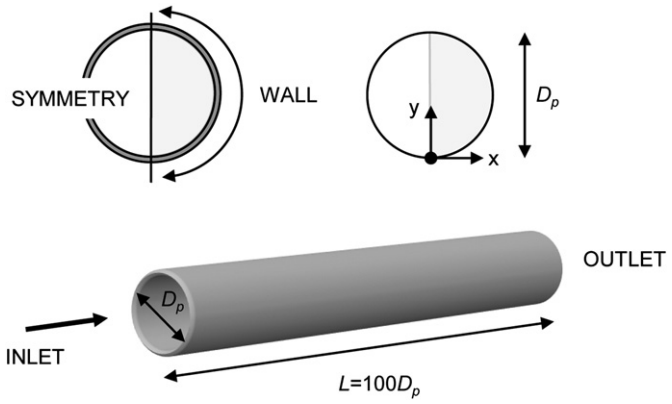

Fig. 3. Computational domain and boundary conditions.

the same velocity distribution is applied to the fluid and the particles ($u^{in}_{z,f} = u^{in}_{z,p}$).

$$u^{in}_{f,z} = u^{in}_{p,z} = V_s \frac{(N+1)(2N+1)}{2N^2}\left(1-\frac{2r}{D_p}\right)^{1/N} \quad N = \frac{1}{\sqrt{f}}$$
$$f = [1.82\log(\mathrm{Re}) - 1.64]^{-2} \quad \mathrm{Re} = \frac{V_s D_p}{\nu} \tag{13}$$

$$k^{in} = V_s^2 \frac{f}{8}\left[1 + \frac{2}{3}\frac{2r}{D_p} + \frac{10}{3}\left(\frac{2r}{D_p}\right)^3\right] \tag{14}$$

$$\varepsilon^{in} = 0.1643\frac{k^{3/2}}{l_m}$$
$$l_m = \frac{D_p}{2}\left[0.14 - 0.08\frac{2r}{D_p} - 0.06\left(\frac{2r}{D_p}\right)^4\right] \tag{15}$$

In Eq. (13), V_s is the superficial velocity of the slurry. The inlet volume fractions of both phases (α_f^{in} and α_p^{in}) are taken as uniformly distributed. At the outlet, the normal gradients of all variables and the value of the pressure are set to zero. The length of the computational domain is $100D_p$ to ensure that fully-developed flow conditions are attained, which typically occurs some $50D_p$ downstream of the inlet, confirming the results of previous workers [10]. At the pipe wall, no slip conditions are imposed to both phases, and the equilibrium wall function of Launder and Spalding [49] for smooth walls is employed to evaluate the velocity component parallel to the wall for the two phases $u^w_{k=f,p}$, the turbulent kinetic energy k^w, and its dissipation rate ε^w in the near wall cells:

$$\frac{u^w_k}{u^*_k} = \frac{1}{\kappa}\ln\left(E\frac{u^*_k y}{\nu}\right) \tag{16}$$

$$k^w = \frac{u^*_f}{\sqrt{C_\mu}} \tag{17}$$

$$\varepsilon^w = C_\mu^{3/4}\frac{k_w^{3/2}}{\kappa y} \tag{18}$$

where: u^*_k is the friction velocity of phase $k = f, p$; $\kappa = 0.41$ is the von Karman constant; E is a roughness parameter, which was set to 8.6 as appropriate for smooth walls; and y is the normal distance of the first grid point from the wall.

2.4. Computational methodology

The general-purpose, commercial CFD code PHOENICS is employed for the numerical solution of the finite-volume analog of the mathematical model described above. This is done by using the built-in Eulerian, two-fluid, Inter-Phase Slip Algorithm (IPSA) of Spalding [38,39] together with user-defined functions and subroutines for implementation of specific constitutive equations and boundary conditions. The calculations are performed following the elliptic-staggered formulation in which the scalar variables are evaluated at the cell centers and the velocity components at the cell faces. Central differencing is employed for the diffusion terms, while the convection terms are discretized using the hybrid differencing scheme of Spalding [56]. The finite-volume equations are solved iteratively by means of the SIMPLEST [50] and IPSA [38,39] algorithms of Spalding. The calculation procedure is organized in a slab-by-slab manner, in which all the dependent variables are solved at the current slab before the solver routine moves to the next slab. The numerical solution procedure requires appropriate relaxation of the field variables to achieve convergence. Inertial relaxation is applied to the momentum equations with a false-time step of 0.01 s, which is the order of the cell convection time. A linear relaxation factor of 0.4 is applied to all other flow variables.

A cylindrical-polar structured mesh was used to discretize the domain. A grid independence study revealed that a grid consisting of 90,000 cells (15 angular by 30 radial by 200 axial) produces a consistent numerical solution. However, it is the disposition of the cells rather than their overall number that is the key feature to guarantee the reliability of the results. In the single-phase flow case, the equilibrium wall function of Launder and Spalding [49] for smooth walls in conjunction with the standard k–ε turbulence model poses strict requirements on the dimensionless wall distance of the first grid point $y^+ = u^* y/\nu$, where u^* is the friction velocity. This law holds in the log law region, and therefore, strictly it may be applied only for y^+ in the range from 30 to about 130. As a consequence, the numerical solution (and, in particular, the computed pressure gradient) is reliable only if the aforementioned condition is satisfied. Fig. 4 depicts the computed pressure gradient versus y^+ for a given set of flow conditions. In the plot, the trend of the white circles, which refer to the single-phase case, confirms that the pressure gradient is predicted inconsistently for $y^+ < 30$.

With a two-fluid model the situation is more complex because the phases are treated as coupled interpenetrating continua, and thus the dependence of the computed pressure gradient on y^+ is more difficult to interpret. With the proposed two-fluid model, in which the equilibrium wall function of Launder and Spalding [49] for smooth walls is applied to both phases, it was judged appropriate to define y^+ with respect to the friction velocity of the fluid phase u^*_f and still satisfy the

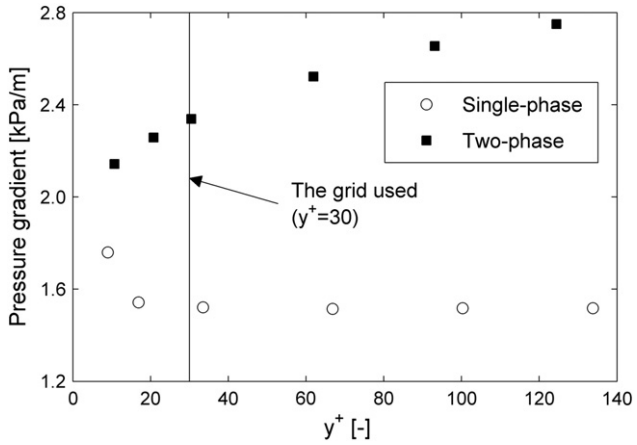

Fig. 4. Computed pressure gradient as a function of the dimensionless distance between the centers of the near wall cells and the pipe wall y^+. The single-phase case is reported too.

constrain $30 < y^+ < 130$. The coupling between the phases influences significantly the dependence of pressure gradient upon y^+, which differs significantly from the single-phase case (Fig. 4). In this work, the mesh was designed in such a way that $y^+ = 30$, which is the smallest possible value consistent with the application of the equilibrium wall function for smooth walls in the single-phase flow case. As illustrated in Messa [46], for a given y^+, further increase in the mesh resolution procured negligible changes in the numerical solution, in terms of all the three main features of interest (pressure gradient, and solid concentration and velocity distributions).

The PHOENICS solver was run until the sum of the absolute residual errors over the whole solution domain is less than 1% of reference quantities based on the total inflow of the variable in question. An additional requirement is that the values of the monitored dependent variables at a selected location do not change by more than 0.1% between subsequent iteration cycles.

The proposed model appears very robust, and is capable of providing a converged steady-state solution within a relatively short computer time. As a rough estimate, about half an hour CPU time is required with a quad-core Intel processor with 2.83 GHz and 8 GB RAM.

3. Results

The numerical model is validated by comparing the results of the simulations against experimental data reported by different authors [7,11,13–15]. The analysis is limited to fully-suspended flows, even if moving-bed flow conditions were marginally addressed in order to establish the overall applicability of the model. Unfortunately, the flow pattern was rarely declared by the experimenters, although in a few cases [14], it could be established rather unquestionably from measurements of the deposition velocity. More frequently, it could be evidenced from the plots of pressure gradient versus slurry velocity, where however the identification of the minimum may be rather confusing. In the experiments of Roco and Shook [11], the flow pattern could be only guessed from the shape of the concentration profile, or from an a priori estimation of the deposition velocity. The comparison focuses on the flow features of main engineering interest, namely the pressure gradient, the solid volume fraction distribution, and the velocity distribution. These features will be addressed in separate sub-sections below.

3.1. Pressure gradient

The capability of the model to predict the pressure gradient of the slurry is discussed first. Fig. 5 compares the predicted pressure gradient – which is depicted as a function of the slurry superficial velocity – with the measured values for the flow conditions listed in Table 1. In all cases, the carrier fluid is water at 20 °C (density = 998.23 kg/m^3; kinematic viscosity = 10^{-6} m^2/s). Unfortunately neither the density of the solid particles nor the pipe roughness is reported in the experiments of Matousek [7]; and so in the simulations the former was set to 2650 kg/m^3, which is the value declared by Gillies et al. [15], and the pipe was regarded as hydraulically smooth. The same assumption holds in the experiments of Gillies et al. [15] and Shaan et al. [14], due to the extremely low pipe roughness to diameter ratio ($\approx 2 \cdot 10^{-5}$). The plots reported in Fig. 5 indicate that the proposed model procures a good estimation of the pressure gradient for fully-suspended flows over a wide range of operating conditions. Conversely, the model is not capable of detecting the minimum in the pressure gradient versus slurry-superficial-velocity curve, which characterizes the transition from fully suspended to bed flows (cases P4 and P6). The same limitation is shared by other two-fluid models available in the literature [23,35]. Moreover, for the same flow conditions P4 and P6, the model overestimates the pressure gradient at high superficial velocity. A possible explanation for such behavior will be provided later.

Fig. 6 shows the parity plot "computed pressure gradient" versus "measured pressure gradient" for all the simulations. The flow conditions include those summarized in Table 1, as well as the additional ones reported in Table 2. In all cases, the flow is fully-suspended, as inferred from the experimental data. Basically for all the flow conditions considered, the model predicts the pressure gradient to within about ±20% of the measured value. Although such a level of accuracy could

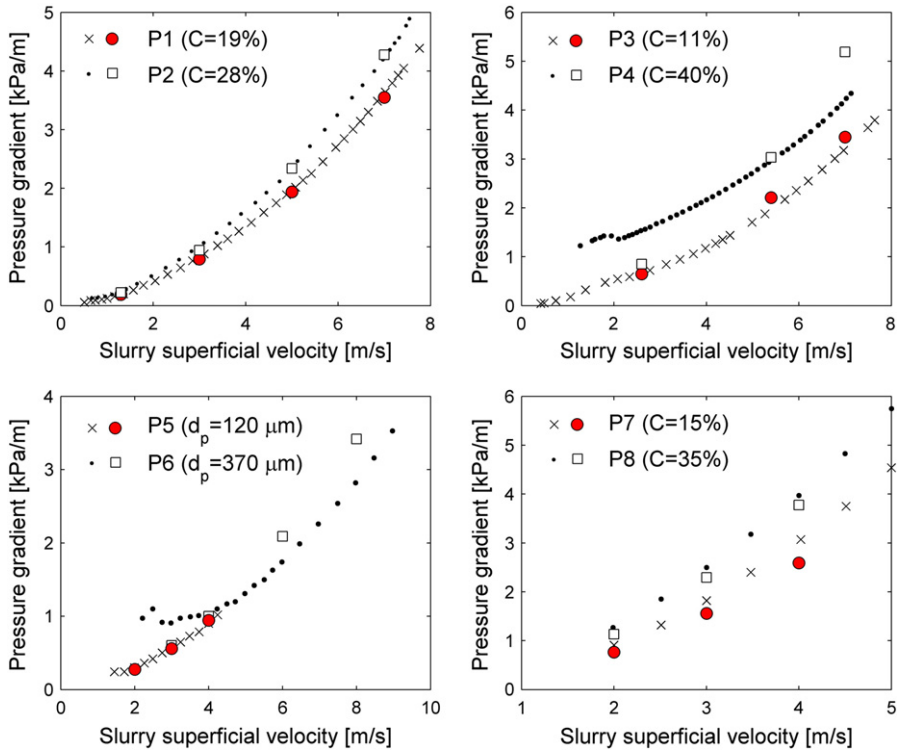

Fig. 5. Pressure gradient versus slurry superficial velocity for the flow conditions reported in Table 1 (× ●: experiments from [7,14,15]; ● □: prediction).

Table 1
Flow conditions considered in the "pressure gradient versus velocity" comparison.

Case ID	Experimenter	D_p [mm]	Particles	ρ_p [kg/m^3]	d_p [μm]	C [%]
P1	Gillies et al. [15]	103.0	Sand	2650	90	19
P2	Gillies et al. [15]	103.0	Sand	2650	90	28
P3	Gillies et al. [15]	103.0	Sand	2650	280	11
P4	Gillies et al. [15]	103.0	Sand	2650	280	40
P5	Matousek [7]	150.0	Sand	–	120	26
P6	Matousek [7]	150.0	Sand	–	370	26
P7	Shaan et al. [14]	53.2	Glass beads	2440	100	15
P8	Shaan et al. [14]	53.2	Glass beads	2440	100	35

Table 2
Additional flow conditions reported in the "parity plot" comparison.

Experimenter	D_p [mm]	Particles	ρ_p [kg/m^3]	d_p [μm]	C [%]
Gillies et al. [15]	103.0	Sand	2650	90	24
Gillies et al. [15]	103.0	Sand	2650	90	33
Gillies et al. [15]	103.0	Sand	2650	280	20
Gillies et al. [15]	103.0	Sand	2650	280	31

be acceptable for many engineering applications, an attempt is now made to investigate more deeply the results in Fig. 6.

For this reason, it is proposed to classify the particles according to their size expressed in wall units, $d_p^+ = u_f^* d_p/\nu$. The quantity $d_p{}^+$ allows comparing the size of the particles to that of the boundary layer, and it depends on both the particle size and the flow conditions (via u_f^*). As sketched in Fig. 7, the particles are referred to as "small" if their size is small compared to the extension of the log law region and "big" otherwise. The threshold value of $d_p{}^+ = 50$ separates the two classes. This value appears rather arbitrary, but it is not very significant in itself because the flow conditions considered refer to either $d_p{}^+ \gg 50$ or $d_p{}^+ \ll 50$. The red-filled points and the white-filled ones in Fig. 6 correspond to "small" and "big" particles respectively. The accuracy of the predictions of the pressure gradient can be related rather clearly to the particle class. In fact, the two-fluid model overestimates the pressure gradient for the "big" particles, while an underestimation is more likely to occur for the "small" ones. If the attention is limited to the latter class, the predictions of pressure gradient basically lie within the interval [−15%, 0] of the measured value, with significant increase of the reliability of the model. Two reasons may contribute to explain the overestimation which characterizes the "big" particles. Firstly, the considerable dimension of the particles compared to the boundary layer thickness may cast doubt on the assumption that the solid phase behaves as a continuum within the log law region, with mean velocity given by the smooth-wall log law of Launder and Spalding [48]. Moreover, the effects of the hydrodynamic lift (not considered in the computations due to the lack of a proper closure model) are enhanced when

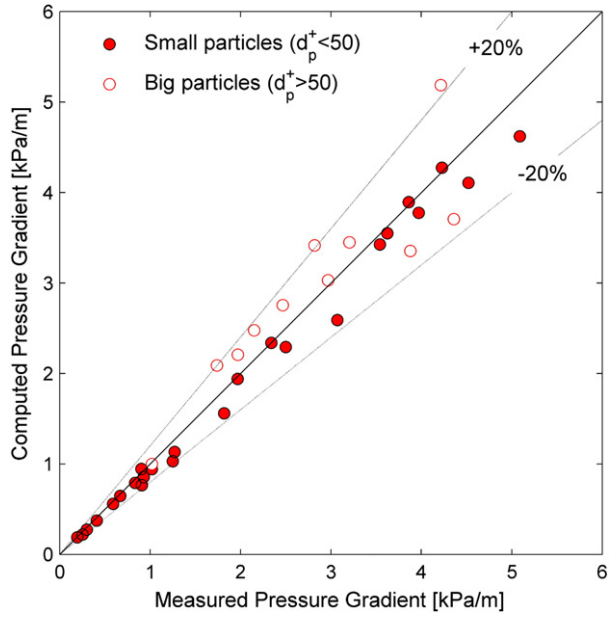

Fig. 6. Parity plot "computed pressure gradient" versus "measured pressure gradient" for all the flow conditions listed in Tables 1 and 2.

the center of the particles lies in the log law region [8], which is precisely the "big" particle case.

3.2. Volume fraction distribution

The predictive capability of the model for simulating the volume fraction distribution is now considered for the flow conditions listed in Table 3, as investigated experimentally by Roco and Shook [11], Gillies et al. [15], and Matousek [7,13]. The pipe is assumed hydraulically smooth even if this hypothesis could be verified only in the experiments of Gillies et al. [15], who reported values of pipe roughness. In the flow conditions investigated by Gillies et al. [15] and Matousek [7,13] the complete suspension of the particles was verified from the plots of pressure gradient versus slurry superficial velocity; while in those of Roco and Shook [11] it was inferred by comparing the slurry velocity with the estimates of the deposition velocity provided by the formula of Wasp [4] (Eq. (1)). The experimental evidence suggests either heterogeneous or pseudo-homogeneous flow. All the data considered for comparison are obtained using gamma-ray absorption methods, which entail errors of the order of only a few percentage points. Since this technique allows measuring chord-average values of solid volume fraction, the comparison between computations and measurements was made in terms of the chord-average solid volume fraction profile (Fig. 2(b)). The results are reported in Fig. 8, in which the data of Matousek [7,13] have error bars indicating the uncertainty declared by the author. The good agreement between computations and measurements indicates the model's ability to predict the volume fraction distribution of fully-suspended slurries over a wide range of operating conditions. As far as the experiments of Matousek [7,13] are concerned, the lack of complete information about the experimental conditions must be taken into account when comparing measurements and predictions, especially in regard to the deviations observed in cases C12 and C15.

3.3. Velocity distribution

The velocity distributions are now considered for the flow conditions summarized in Table 4, as investigated experimentally by Roco and Shook [11] and Gillies et al. [15]. The hypothesis of hydraulically smooth pipes, verified in the experiments of Gillies et al. [15], could

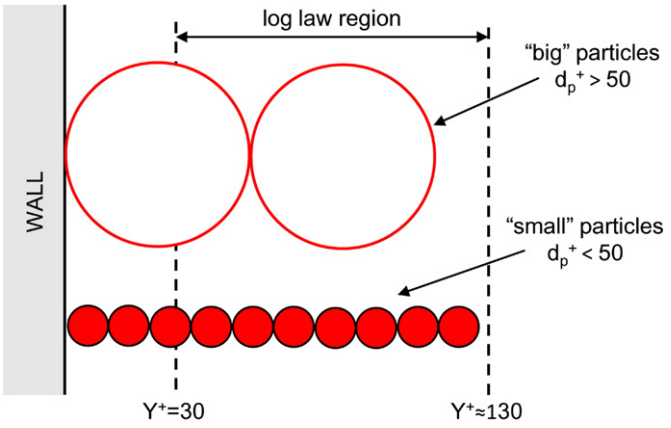

Fig. 7. Classification between "small" and "big" particles.

Table 3
Solid volume fraction distribution: flow conditions considered for comparison.

Case ID	Experimenter	D_p [mm]	Particles	ρ_p [kg/m^3]	d_p [μm]	C [%]	V_s [m/s]
C1	Roco and Shook [11]	51.5	Sand	2650	165	9	3.78
C2	Roco and Shook [11]	51.5	Sand	2650	165	19	4.17
C3	Roco and Shook [11]	51.5	Sand	2650	165	29	4.33
C4	Gillies et al. [15]	103.0	Sand	2650	90	19	3.00
C5	Gillies et al. [15]	103.0	Sand	2650	90	24	3.00
C6	Gillies et al. [15]	103.0	Sand	2650	90	28	3.00
C7	Gillies et al. [15]	103.0	Sand	2650	90	33	3.00
C8	Gillies et al. [15]	103.0	Sand	2650	280	11	5.40
C9	Gillies et al. [15]	103.0	Sand	2650	280	20	5.40
C10	Gillies et al. [15]	103.0	Sand	2650	280	30	5.40
C11	Gillies et al. [15]	103.0	Sand	2650	280	41	5.40
C12	Matousek [7,13]	150.0	Sand	–	120	26	2.00
C13	Matousek [7,13]	150.0	Sand	–	120	35	2.00
C14	Matousek [7,13]	150.0	Sand	–	120	34	6.00
C15	Matousek [7,13]	150.0	Sand	–	370	26	6.00

only be presumed for the data of Roco and Shook [11]. Likewise, from analysis of the solid–volume-fraction distribution, the effectiveness of the turbulence in keeping the solids fully suspended was verified for the flow conditions of Gillies et al. [15], who reported plots of pressure gradient versus slurry velocity, but only inferred for the data of Roco and Shook [11] by verifying that the slurry velocity is much higher than the deposition velocity calculated from Eq. (1). Since both experimenters used the electrical probe developed at the University of Saskatchewan [25], which provides values of the particle velocity, the comparison between experiments and computations was made with respect to the axial particle velocity profile along the vertical diameter. Fig. 9 shows the results of this comparison, and it can be seen that the model predicts velocity profiles in rather good agreement with the experimental data. In particular, the model is capable of reproducing the asymmetry of the profile, in which the maximum velocity is positioned above the pipe axis (cases V2, V3, and V4). Other previous two-fluid models [33,36] were also able to reproduce this characteristic feature of the flow, but no comparison with the measurements was reported. On the other hand, the application-specific model of Roco and Shook [11] is experimentally validated with respect to solid volume fraction and velocity measurements, but not with respect to the pressure gradient data.

4. Conclusion

A mathematical model has been described for the simulation of fully-suspended slurry flows in horizontal pipes. The model is based on an Eulerian–Eulerian approach, and uses the Inter-Phase Slip Algorithm (IPSA) of Spalding [38,39]. The combined use of existing modeling strategies, never previously employed together for the prediction of slurry flows in horizontal pipes, allows a reliable prediction of these flows. Phase diffusion fluxes are introduced in all conservation equations to account for the turbulent dispersion of particles. The mixture viscosity approach is employed to model the effect of the presence of multiple particles on interfacial momentum transfer. A wall function is used to model the additional wall shear stress due to interactions between the particles and the wall. The model proved robust and numerically stable, and converged steady-state solutions were attained within a relatively short computer time. In comparison with similar models, the present model reveals better performance in terms of numerical

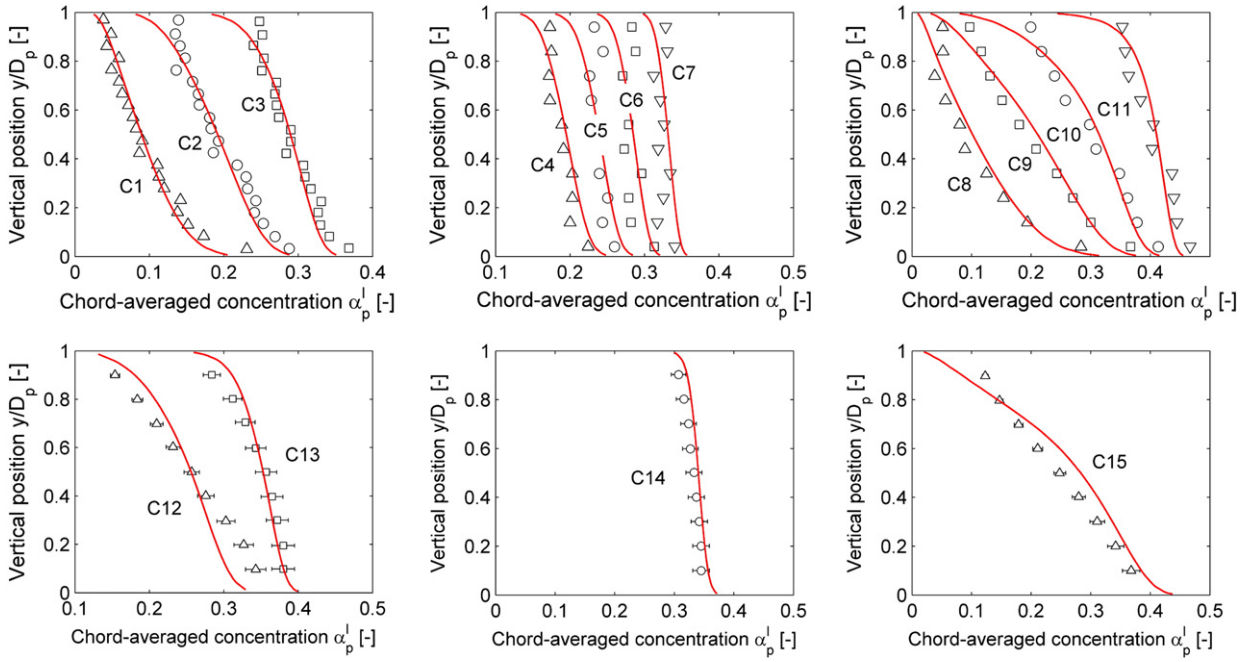

Fig. 8. Chord-average solid volume fraction profile for the flow conditions reported in Table 3 (△□○▽: experiments from [7,11,14,15]; —— : prediction).

Table 4
Velocity distribution: flow conditions considered for comparison.

Case ID	Experimenter	D_p [mm]	Particles	ρ_p [kg/m^3]	d_p [μm]	C [%]	V_s [m/s]
V1	Roco and Shook [11]	51.5	Sand	2650	165	9	3.78
V2	Roco and Shook [11]	50.7	Sand	2650	520	12	3.20
V3	Roco and Shook [11]	50.7	Sand	2650	520	11	4.00
V4	Gillies et al. [15]	103.0	Sand	2650	90	20	1.33
V5	Gillies et al. [15]	103.0	Sand	2650	90	20	2.00
V6	Gillies et al. [15]	103.0	Sand	2650	90	20	3.00

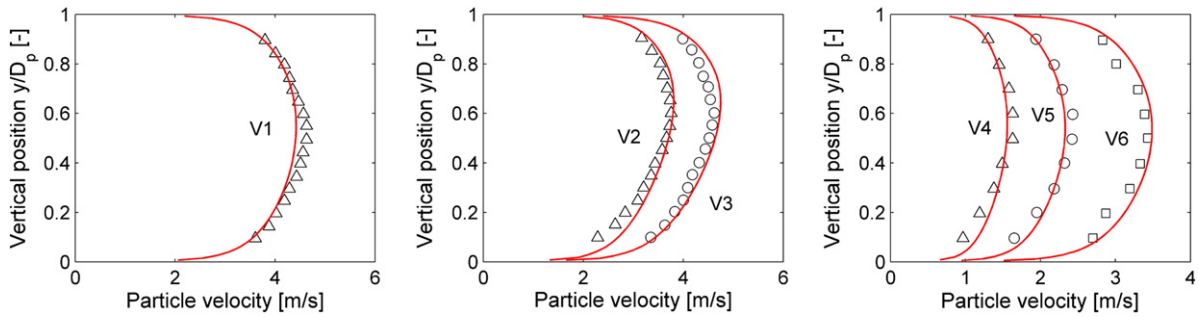

Fig. 9. Particle velocity profile along the vertical diameter for the flow conditions reported in Table 4 (△□○: experiments from [11,15]; —— : prediction).

efficiency, quality of the solution, range of applicability, and possibly better agreement with the experimental evidence.

The model has been validated by comparison with experimental data from several authors [7,11,13–15] over a large range of operating conditions: pipe diameter between 50 and 150 mm; particles of different materials (glass beads and sand) and sizes (90 to 520 μm) at mean delivered concentration up to 40% by volume; and slurry superficial velocity between 1 and 7 m/s.

The model proved capable of providing estimations of the pressure gradient within about ±20% of the measured values. Further analysis of the results revealed that the range of deviation can be reduced to about [−15%, 0] of the measured value, if the particles are "small" compared to the extension of the log law region (Figs. 6–7). The predicted chord-average solid–volume-fraction distribution agreed with the experimental evidence for both pseudo-homogeneous and heterogeneous flows (Fig. 8). The agreement was also good for the vertical particle velocity profile (Fig. 9); in particular, the model was able to replicate the measured asymmetry of the profile due to gravitational stratification.

Acknowledgments

This work has been supported by Regione Lombardia and CILEA Consortium through a LISA Initiative (Laboratory for Interdisciplinary Advanced Simulation) 2010 grant [link: http://lisa.cilea.it]. The authors acknowledge Dr. Randy Gillies of Saskatchewan Research Council for making his experimental data available for use in this research.

Appendix A. Supplementary data

References

[1] P. Doron, D. Barnea, Flow pattern maps for solid–liquid flow in pipes, Int. J. Multiphase Flow 22 (2) (1996) 273–283.
[2] B.E. Albunaga, Slurry Systems Handbook, McGraw-Hill, New York, 2002.
[3] S.M. Pecker, S.S. Helvaci, Solid–Liquid Two-phase Flow, Elsevier, Amsterdam, 2008.
[4] E.J. Wasp, J.P. Kenny, R.L. Gandhi, Solid Liquid Flow Slurry Pipeline Transportation, Trans. Tech. Publication, Clausthal, Germany, 1977.
[5] C.A. Shook, A.S. Bartosik, Particle–wall stresses in vertical slurry flows, Powder Technol. 81 (2) (1994) 117–124.
[6] V. Matousek, Research developments in pipeline transport of settling slurries, Powder Technol. 156 (1) (2005) 43–51.
[7] V. Matousek, Pressure drops and flow patterns in sand–mixture pipes, Exp. Therm Fluid Sci. 26 (6–7) (2002) 693–702.
[8] K.C. Wilson, A. Sellgren, Interaction of particles and near-wall lift in slurry pipelines, J. Hydraul. Eng. 129 (1) (2003) 73–76.
[9] K.C. Wilson, R.S. Sanders, R.G. Gillies, C.A. Shook, Verification of the near-wall model for slurry flow, Powder Technol. 197 (3) (2010) 247–253.
[10] J. Ling, P.V. Skudarnov, C.X. Lin, M.A. Ebadian, Numerical investigations of solid–liquid slurry flows in a fully developed flow region, Int. J. Heat Fluid Flow 24 (3) (2003) 389–398.
[11] M.C. Roco, C.A. Shook, Modeling of slurry flow: the effect of particle size, Can. J. Chem. Eng. 61 (4) (1983) 494–503.
[12] J.M. Colwell, C.A. Shook, The entry length for slurries in horizontal pipeline flow, Can. J. Chem. Eng. 66 (5) (1988) 714–720.
[13] V. Matousek, Concentration distribution in pipeline flow of sand–water mixtures, J. Hydrol. Hydromech. 48 (3) (2000) 180–196.
[14] J. Shaan, R.J. Sumner, R.G. Gillies, C.A. Shook, The effect of particle shape on pipeline friction for Newtonian slurries of fine particles, Can. J. Chem. Eng. 78 (4) (2000) 717–725.
[15] R.G. Gillies, C.A. Shook, J. Xu, Modelling heterogeneous slurry flow at high velocities, Can. J. Chem. Eng. 82 (5) (2004) 1060–1065.
[16] P.V. Skudarnov, C.X. Lin, M.A. Ebadian, Double-species slurry flow in a horizontal pipeline, ASME, J. Fluids Eng. 126 (1) (2004) 125–132.
[17] C. Kim, M. Lee, C. Han, Hydraulic transport of sand–water mixtures in pipelines. Part I. Experiment, J. Mech. Sci. Technol. 22 (12) (2008) 2534–2541.
[18] D.R. Kaushal, Y. Tomita, Comparative study of pressure drop in multisized particulate slurry flow through pipe and rectangular duct, Int. J. Multiphase Flow 29 (9) (2003) 1473–1487.
[19] D.R. Kaushal, K. Sato, T. Toyota, K. Funatsu, Y. Tomita, Effect of particle size distribution on pressure drop and concentration profile in pipeline flow of highly concentrated slurry, Int. J. Multiphase Flow 31 (7) (2005) 809–823.
[20] D.R. Kaushal, Y. Tomita, Experimental investigation for near-wall lift of coarser particles in slurry pipeline using γ-ray densitometer, Powder Technol. 172 (3) (2007) 177–187.
[21] U. Kumar, R. Mishra, S.N. Singh, V. Seshadri, Effect of particle gradation on flow characteristics of ash disposal pipelines, Powder Technol. 132 (1) (2003) 39–51.
[22] Y.Y. Jiang, P. Zhang, Numerical investigation of slush nitrogen flow in a horizontal pipe, Chem. Eng. Sci. 73 (2012) 169–180.
[23] Y.Y. Jiang, P. Zhang, Pressure drop and flow pattern of slush nitrogen in a horizontal pipe, AIChE J (2012), http://dx.doi.org/10.1002/aic.13927.
[24] H. Nasr-el-Din, C.A. Shook, M.N. Esmail, Isokinetic probe sampling from slurry pipelines, Can. J. Chem. Eng. 62 (2) (1984) 179–185.
[25] N.P. Brown, C.A. Shook, J. Peters, D. Eyre, A probe for point velocities in slurry flows, Can. J. Chem. Eng. 61 (4) (1983) 597–602.
[26] R.C. Chen, Experimental and Numerical Studied of Solid–Liquid Multiphase Flow in Pipes, PhD thesis Case Western Reserve University, 1991.
[27] S. Kumar, M.P. Dudukovic, B.A. Toseland, Measurement Techniques for Local and Global Fluid Dynamic Quantities in Two and Three Phase Systems, Technical Report, Federal Energy Technology Center, Morgantown, West Virginia, 1998.

[28] P. Doron, D. Granica, D. Barnea, Slurry flow in horizontal pipes — experimental and modeling, Int. J. Multiphase Flow 13 (4) (1987) 535–547.
[29] R.G. Gillies, C.A. Shook, Modelling high concentration settling slurry flows, Can. J. Chem. Eng. 78 (4) (2000) 709–716.
[30] P. Doron, D. Barnea, A three layer model for solid–liquid flow in horizontal pipes, Int. J. Multiphase Flow 19 (6) (1993) 1029–1043.
[31] P. Doron, D. Barnea, Pressure drop and limit deposit velocity for solid–liquid flow in pipes, Chem. Eng. Sci. 50 (10) (1995) 1595–1604.
[32] V. Matousek, Predictive model for frictional pressure drop in settling-slurry pipe with stationary deposit, Powder Technol. 192 (3) (2009) 367–374.
[33] D.R. Kaushal, T. Thinglas, Y. Tomita, S. Juchii, H. Tsukamoto, CFD modeling for pipeline flow of fine particles at high concentration, Int. J. Multiphase Flow 43 (2012) 85–100.
[34] R.C. Chen, Analysis of homogeneous slurry pipe flow, J. Mar. Sci. Technol. 2 (1) (1994) 37–45.
[35] L. Chen, Y. Duan, W. Pu, C. Zhao, CFD simulation of coal-water slurry flowing in horizontal pipelines, Korean J. Chem. Eng. 26 (4) (2009) 1144–1154.
[36] K. Ekambara, R.S. Sanders, K. Nandakumar, J.H. Masliyah, Hydrodynamic simulation of horizontal slurry pipeline flow using ANSYS-CFX, Ind. Eng. Chem. Res. 48 (17) (2009) 8159–8171.
[37] S.K. Lahiri, K.C. Ghanta, Slurry flow modeling by CFD, CI&CEQ, 16 (4) (2010) 295–308.
[38] D.B. Spalding, Numerical computation of multi-phase fluid flow and heat transfer, in: C. Taylor, K. Morgan (Eds.), Recent Advances in Numerical Methods in Fluids, Pineridge Press Limited, Swansea, UK, 1980, pp. 139–168.
[39] D.B. Spalding, IPSA 1981: new developments and computed results, CFDU Report HTS/81/2, Imperial College, London, 1981.
[40] A.D. Burns, T. Frank, I. Hamill, J.M. Shi, The Favre averaged drag model for turbulent dispersion in Eulerian multi-phase flows, Proc. 5th International Conference on Multiphase Flow ICMF2004, 2004, Paper No. 392.
[41] J.S. Shirolkar, C.F.M. Coimbra, M.Q. McQuay, Fundamental aspects of modelling turbulent particle dispersion in dilute flows, Prog. Energy Combust. Sci. 22 (4) (1996) 363–399.
[42] X. Chen, Y. Li, X. Niu, M. Li, D. Chen, X. Yu, A general two-phase turbulent flow model applied to the study of sediment transport in open channels, Int. J. Multiphase Flow 37(9), 1099–1108
[43] M. Ishii, K. Mishima, Two-fluid model and hydrodynamic constitutive relations, Nucl. Eng. Des. 82 (2–3) (1984) 107–126.
[44] J.N. Chung, T.R. Troutt, Simulation of particle dispersion in an axisymmetric jet, J. Fluid Mech. 186 (1) (1988) 199–222.
[45] L. Shiller, A. Naumann, A drag coefficient correlation, Z. Ver. Dtsch. Ing. 77 (1935) 318–320.
[46] G.V. Messa, Two-fluid Model for Solid–Liquid Flows in Pipeline Systems, PhD Thesis Politecnico di Milano University, Milano, Italy, 2013.
[47] M. Mooney, The viscosity of a concentrated suspension of spherical particles, J. Colloid Sci. 6 (2) (1951) 162–170.
[48] S. Antal, R. Lahey, J. Flaherty, Analysis of phase distribution in fully-developed laminar bubbly two phase flow, Int. J. Multiphase Flow 17 (5) (1991) 635–652.
[49] B.E. Launder, D.B. Spalding, The numerical computation of turbulent flows, Comput. Meth. Appl. Mech. Eng. 3 (1974) 269–289.
[50] D.B. Spalding, Mathematical modelling of fluid-mechanics, heat-transfer and chemical-reaction processes: a lecture course, CFDU Report HTS/80/1, Imperial College, London, 1980.
[51] D.B. Spalding, PHOENICS: a general-purpose computer program for multi-dimensional one- and two-phase flow, CFDU Report HTS/81/11, Imperial College, London, 1981.
[52] S.E. Elghobashi, T.W. Abou-Arab, A two-equation turbulence model for two-phase flows, Phys. Fluids 26 (1983) 931–938.
[53] Y. Sato, K. Sekoguchi, Liquid velocity distribution in two-phase bubbly flow, Int. J. Multiphase Flow 2 (1) (1975) 79–95.
[54] R.I. Issa, P.J. Oliveira, Assessment of a particle–turbulence interaction model in conjunction with an Eulerian two-phase flow formulation, Proc. 2nd Int. Symp. on Turbulence, Heat and Mass Transfer, 1997, pp. 759–770.
[55] H. Schlichting, Boundary Layer Theory, McGraw-Hill, New York, 1960.
[56] D.B. Spalding, A novel finite-difference formulation for differential expressions involving both first and second derivatives, Int. J. Numer. Methods Eng. 4 (4) (1972) 551–559.